LAWRENCE
LIVERMORE
NATIONAL
LABORATORY

LLNL-JRNL-401824

Melting line and fluid structure factor of oxygen up to 24 GPa

G. Weck, P. Loubeyre, J. Eggert, M. Mezouar, M. Hanfland

February 29, 2008

Physical Review B

Updated October 14, 2003

,

Melting line and fluid structure factor of oxygen up to 24 GPa.

Gunnar Weck and Paul Loubeyre

DIF/DPTA/SPMC, CEA, 91680 Bruyères–le–Châtel, France

Jon H. Eggert

Lawrence Livermore National Laboratory,

P.O. Box 808, Livermore, California 94550, USA

Mohamed Mezouar and Michael Hanfland

European Synchrotron Radiation Facility, BP 220, 38043 Grenoble, France

(Dated: March 26, 2007)

Abstract

Using synchrotron x-ray diffraction and Raman spectroscopy, we have measured the structural properties of dense fluid O_2 up to 24 GPa. A quantitative evolution with pressure of the structure factor of a low-Z molecular fluid is obtained here for the first time under pressure. No evidence of molecular association is observed here in contrast to what has been observed in the cryo O_2 fluid or in the solid above 12 GPa. The melting curve, which can evidence structural changes in the fluid or the solid, has also been measured up to 750 K by direct visualization of the solid-fluid equilibrium. No unusual behavior is observed hence invalidating a previous report.

PACS numbers: 62.50.+p, 61.20.-p, 61.25.Em, 61.10.Nz

I. INTRODUCTION

Remarkable structural changes have recently been disclosed at high pressure in simple molecular solids, more particularly in H_2[1], O_2[2], N_2[3] or CO_2[4]. Similarly, the combining effects of density and disorder should also produce a variety of interesting transformations in dense molecular fluids such as polymerization, dissociation or metallization. Up to now, measurements in these dense molecular fluids have been achieved by dynamical compression. Single-shock Hugoniot data have been used to constrain their equation of state and to adjust effective pair interactions. Also, metallization of fluid H_2, O_2[5] and N_2[6] has been obtained by reverberating shock wave techniques. Yet, the fundamental questions on the nature of the structural changes at a microscopic level in these dense molecular fluids would be extremely hard to answer in dynamical measurements.

The major progress in the structural study of molecular solids under pressure have been achieved by a combination of the confinement of the sample in the diamond anvil cells (DAC) and the use of third generation synchrotron sources. But similar structural studies in simple molecular fluids at high pressure, hence at high temperature, have been hampered by three factors: the difficulty of producing stable thermodynamical conditions for fine measurements due to the instability and chemical attack of the gasket or the breaking of the anvils by the molecular diffusion in the diamond; the lack of a well established pressure gauge above 700K; the difficulty of measuring high quality structure factor in low-Z fluids confined in diamond anvil cells because the low scattering intensity of the sample is mostly hidden by the large background signal generated by the diamond anvils. We present here the first structural study of a low-Z molecular fluid at high pressure. That was made possible by a combination of improved sample confinement, the use of the boron nitride pressure gauge[7] and particularly a recently described method to perform quantitative structure factor measurements of high pressure fluids in a DAC by synchrotron x-ray diffraction.

Fluid O_2 is a good candidate for observing interesting structural changes at high pressure. First, metallization has been observed in the solid above 96 GPa and above 120 GPa in the fluid. That is rather surprising since one would expect, as observed in H_2 and N_2[6] and as calculated from first principles simulations[8], disorder or dissociation effects to lead to a lower pressure of metallization in the fluid than in the ordered solid. DAC structural measurements in the fluid may help to clarify this discrepancy. Structure factor of fluid

O_2 at low temperature presents a shoulder at 4 $Å^{-1}$ which is the signature of long-living O_4 molecular units[9]. Recently, the formation of O_8 molecular units in the solid above 12 GPa has been demonstrated by single crystal x-ray diffraction[2]. A main motivation of the present study is to observe whether or not a similar association of oxygen molecules exist in the dense fluid within the same pressure range.

The article is organized as follows. In section II, we describe the sample confinement and the P-T metrology used. In section III, we present a new determination of the melting line up to 750 K because it is the boundary limit of the fluid domain, where density induced structural changes in the fluid are expected to be maximized. In section IV, the Raman measurement of the vibron O_2 mode indicate that over the P-T range of this study the intramolecular bonding of the O_2 molecule is hardly changing. In section V, the evolution with density of the structure factor of fluid O_2 is presented. In section VI, a comparison with a molecular dynamic simulation performed with the effective pair potential derived from shock wave data shows that the observed fluid has almost uncorrelated molecular orientation. Concluding remarks are presented in section VII.

II. SAMPLE AND METROLOGY

Oxygen samples were loaded cryogenically into membrane diamond-anvil cells equipped with flat culets greater than 300 μm in diameter. To prevent possible chemical reaction between oxygen and the rhenium gasket, the sample was isolated from the gasket by a 10 μm thick ring of gold, as used previously for the measurement of the melting curve of H_2[10]. The typical sample size was about 100 μm in diameter. Before each experiment, the absence of nitrogen in the sample was checked by Raman scattering. We observed that the diffusion of oxygen in the diamond anvil is greatly enhanced above 650 K in the fluid phase near melting pressure. This oxygen diffusion causing the breakage of anvils could be stopped by using Al_2O_3 coated anvils. Six experiments were performed with the technique of the resistive heating gasket to generate high temperatures. These experiments were performed under vacuum. The temperature regulation was performed with the help of a K thermocouple fixed to the base of the diamond. Pressure and temperature were measured in-situ by using either ruby-gold or ruby-samarium crossed gauges[11]. In a last experiment dedicated to the extension of the melting curve above 600K, the whole cell was externally heated in an

Ar/H_2 atmosphere. In this experiment the temperature could be directly measured with the help of a thermocouple in contact with the diamond anvil close to the sample chamber and the pressure was determined both with the ruby, samarium luminescence gauges and the recently calibrated c-BN Raman gauge[7]. As it will be seen below, the reproducibility and the excellent agreement between the various measurements of the melting curve using different gauges give us confidence in the accuracy of our estimation of the P-T conditions of the oxygen sample in the present study.

The Raman setup at the laboratory is a 1.3 m focal length Jarell-Ash spectrograph equipped with 1800-gr/mm grating coupled with a LN_2 cooled CCD from Princeton instrument leading to a typical dispersion of 14 nm over the 1024 pixels of the CCD. This setup was also used to measure the ruby and $SrB_4O_7 : Sm^{2+}$ luminescence spectra. The wavelength calibration of the spectrograph was performed before each acquisition with the spectral lines of a krypton lamp.

The angle-dispersive X-ray diffraction experiments were performed on the ID09 and ID30 beamlines at the ESRF. The cell was equipped with boron seats in order to obtain large X-ray aperture ($\pm 37°$). We used a doubly focused monochromatic beam of diameter 30 μm and energy E = 33 keV or E = 29.5 keV . The scattered photons were collected by an image-plate MAR345 detector. The diffraction patterns were integrated with the FIT2D computer code[12].

III. THE MELTING CURVE

The melting curve is the thermodynamic boundary line of the fluid domain. Obviously, at a given temperature, the density-induced structural changes in the fluid will be maximum near this line. But also, an unusual behavior of the melting curve can reveal interesting structural changes in the fluid, such as in phosphorous with the maximum on the melting curve associated to a first order structural transition in the fluid[13]. An unusual steep increase of the melting curve of oxygen has been previously reported above 620 K[14]. This sharp rise has been ascribed entirely to the existence of a more entropic solid phase along the melting line. However structural changes of the fluid might also contribute to such a rapid rise of the melting temperature. Two sets of measurements were performed to determine the melting curve of pure oxygen (see figure 1). In the first set (3 experiments), the sample

was heated with the technique of the resistive gasket[15] and the pressure and temperature was determined in-situ with the help of the ruby and $SrB_4O_7 : Sm^{2+}$ luminescence gauges. The maximum temperature reached during these experiments was 675 K, since limited by diamond breakages. In a last experiment (between 300 K and 720 K), using coated diamond anvils, the whole cell was heated with an external oven. The temperature was measured with a K-thermocouple fixed to the diamond and we used either the $SrB_4O_7 : Sm^{2+}$ luminescence or the c-BN phonon to determine the pressure. The temperature gradient measured between the heater and the thermocouple near the sample was less than 10 K at 710 K. The P-T melting data have been measured when a stable solid-fluid equilibrium was optically observed, as shown on the photograph in the inset of figure 1. Our melting data are given in table 1 and shown in figure 1. Up to 750 K, the melting temperature of oxygen is a monotonic increasing function of pressure. A least square fit to a Simon equation reproduces our whole data set within the experimental uncertainty and gives:

$$T = ((P + 2.223)/0.0119)^{(1/1.1374)} \quad (1)$$

Up to 620 K, the present melting curve is in excellent agreement with the previous measurement of Yen et al.[16] and Santoro et al.[14] But no sharp increase of the melting curve is detected above 620 K as reported by Santoro et al.[14], although the equilibrium of the fluid with the new solid phase η has been characterized by Raman measurements and x-ray diffraction. We believe that this discrepancy is due to the method used to determine the melting point in this previous work (we have observed that strong pressure variations can arise at melting. Hence, the P-T measurements have to be made when a stable S+F equilibrium is visualized). Three different solid phases have been observed along the melting curve by going up in pressure, β, ε and η, with no visible effect on the melting curve within present experimental accuracy. That is a little surprising though since important structural changes exist at least between the β and ϵ phases. Could there be somehow a compensation of the effect of structural changes in the solid along the melting curve by associated structural changes in the fluid? The structural study of solid oxygen along its melting curve is under progress. We focus here below on the structural changes in the fluid phase.

TABLE I: Eperimental melting points of oxygen determined in this work (T_{melt} in K and P_{melt} in GPa)

P_{melt}	T_{melt}	P_{melt}	T_{melt}	P_{melt}	T_{melt}
5.40	296.0	8.21	389.7	11.82	504.5
5.40	296.0	8.32	392.6	12.03	505.2
5.69[a]	296.0	8.40	395.3	12.11	512.6
5.87	310.3	8.50	399.4	12.12[a]	522.0
6.06	313.4	8.63	401.9	12.16	507.6
6.32	324.9	8.70	407.2	12.27	523.5
6.34	324.4	8.78	411.7	12.50	525.7
6.40	326.1	8.91	410.5	12.73	526.4
6.46	328.5	8.96	417.0	13.05	544.8
6.57	334.3	9.00	407.1	13.32	554.5
6.57	328.4	9.09	418.5	13.37	553.9
6.61	332.5	9.29	416.9	13.61	563.5
6.65	335.9	9.39	422.5	14.01[a]	573.0
6.73	340.5	9.43[a]	420.0	14.12	571.2
6.82	335.6	9.64	432.5	14.45	576.0
6.84	343.3	9.94	448.2	14.72	586.4
6.85	344.1	10.42	455.3	15.02	598.6
6.94	343.9	10.45	464.4	15.29	611.4
6.96	343.3	10.50	459.6	15.56[a]	624.0
7.04	345.6	10.72	475.0	15.92	617.8
7.10	350.2	11.05[a]	477.0	15.94	639.6
7.20	351.2	11.23	482.5	16.28	634.7
7.33	354.8	11.24	489.3	16.48[a]	653.0
7.38	357.6	11.26	483.6	16.63	640.1
7.90	370.6	11.26[a]	477.0	17.50[a]	693.0
8.02	379.8	11.49	493.1	17.96[a]	706.0
8.13	380.8	11.76	496.6	19.60[b]	745.0

[a]pressure determined with the BN gauge

[b]Melting point obtained during the vibron experiment

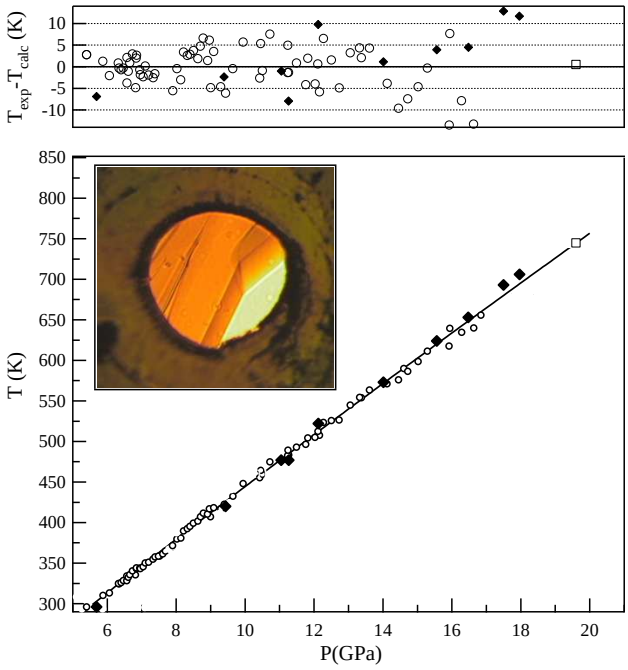

FIG. 1: Oxygen Melting Curve. Two sets of measurements are presented. First set: with the ruby-samarium cross-gauges (○). Second set: with a the c-BN Raman gauge coupled to a thermocouple in contact with the anvil(⧫). The full line correspond to a least square fit of our measurements with a Simon equation. The picture correspond to a solid-fluid equilibrium at T=719 K and P= 18.8 GPa

IV. RAMAN MEASUREMENT

Raman spectroscopy has been extensively used to probe structural changes in the solid phase. In particular, the pressure evolution of the vibron frequency can be used to detect structural changes through discontinuity or change of slope. Furthermore, the vibron mode is the signature of the intramolecular bonding and chemical changes under pressure can also be revealed through large variation of the vibron mode frequencies. We have measured the evolution of the vibron frequency with pressure in the fluid phase at 300 K and 745 K up to solidification (see figure 2). Our data at 300K are in good agreement with the previous determinations of Nicol et al.[17] and Akahama et al.[18]. In fact, the two previous determinations differ by a shift of 3 cm^{-1} and our determination falls exactly in between. At a given pressure, the vibron mode is seen to shift to lower frequency with high temperature. This shift is interpreted as due to the sole density effect. In the inset of figure 2, the

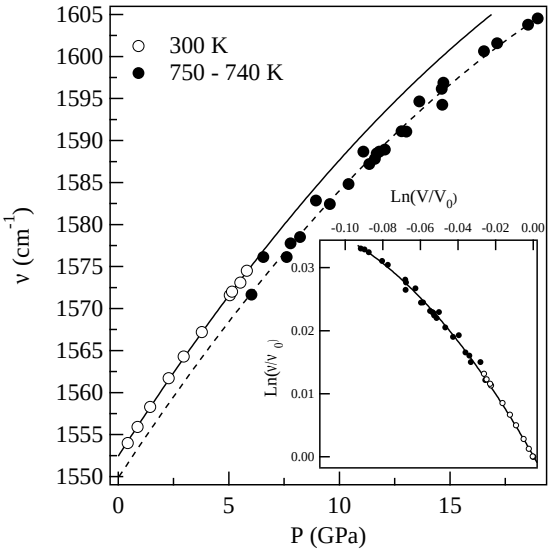

FIG. 2: Pressure evolution of the vibron frequency measured up to the solidification at 300 K (open symbol) and at 745 K (full symbol). Inset: Frequency shift of the vibron versus volume on a logarithmic scale at 300 K (open symbol) and 750 K (full symbol).

frequency shift is given in a Gruneisen plot, i.e frequency versus volume on a logarithmic scale. The volume of the fluid was calculated with an analytical equation of state proposed by Belonoshko et al.[19]. All the data point falls on the same curve. Consequently, following the interpretation of Akahama et al. at 300 K, the pressure dependence of the vibron frequency at 750 K is due also to the solvent shift. The intramolecular bonding is thus hardly perturbed in this fluid domain. This input is used below in the analysis of the x-ray diffraction.

V. X-RAY DIFFRACTION

A major difficulty with liquid diffraction in the diamond anvil cell is that the background signal originating from the diamond anvils, many times as thick as the sample, dominates the diffuse scattering of the liquid sample under pressure, specially for low-Z systems. Scattering from diamond anvils takes the form of: i) Bragg scattering which can be easily removed either by digitally masking the image integration or by rotating the DAC; ii) Compton scattering which is assumed to be independent of pressure and temperature; iii) Temperature diffuse scattering which is far more insidious due to its temperature dependence and anisotropy.

The proper determination of the reference background spectra is probably the most difficult aspect of making and analyzing these liquid measurements. The general method used to extract structure factors and radial distribution functions from X-ray data has been extensively described in a precedent paper[20]. This analysis is applicable to both atomic and molecular fluids. It is applied here for the first time to extract the structural data of a molecular fluid over a large pressure domain. We will recall below few equations as a guide of the essential steps of the measurement and the analysis. But we refer to our previous paper for the full details of this complex analysis.

The different contributions to the measured intensity, $I^{meas}(Q)$, can be separated as follow:

$$I^{meas}(Q) = T(Q)I^{samp}(Q) + sI^{bkgd}(Q) \tag{2}$$

where $T(Q)$ is the DAC transmission calculated from the DAC geometry and absorption coefficients, $I^{bkgd}(Q)$ is the empty-cell background scattering. $I^{bkgd}(Q)$ was generally taken at the end of the experiment after unloading the cell but for the highest pressure points near the melting line, an alternative method was used involving the use of a solid-sample background at nearby thermodynamical conditions. s is the scale factor between $I^{bkgd}(Q)$ and $I^{meas}(Q)$. The last term, $I^{samp}(Q)$, is the sample scattering which can be written as a sum of two different contributions, $I^{coh}(Q)$ and $I^{incoh}(Q)$ respectively the coherent and incoherent(Compton) scattering.

$$I^{samp}(Q) = \frac{1}{N\alpha}\left[I^{coh}(Q) + NI^{incoh}(Q)\right] \tag{3}$$

Here α is the normalization factor to write the sample scattering into atomic units. Finally, the radial distribution function $g(r)$ is related to the coherent intensity through the Fourier transform of the structure factor as follows:

$$S(Q) \equiv \frac{I^{coh}(Q)}{Nf^2(Q)} \tag{4}$$

and

$$F(r) \equiv 4\pi r\rho_0\left[g(r) - 1\right] = \frac{2}{\pi}\int_0^\infty Q(i(Q))\sin(Qr)dQ, \tag{5}$$

Where $f(Q)$ is the atomic form factor, ρ_0 is the atomic density, S(Q) is the liquid structure factor and $i(Q) = S(Q) - 1$. $f(Q)$ and $I^{incoh}(Q)$ are computed using the analytic atomic formulae given by Hajdu,[21].

It follows from the above equations that, in order to extract $S(Q)$ and $g(r)$, we need to determine the α and s coefficients. On one hand, the normalization factor, α , can be obtain with the help of the Krogh-Moe and Norman method[22, 23]

$$\alpha = \frac{-2\pi^2\rho_0 + \int_0^{Q_{max}} \left[\frac{I^{incoh}(Q) + Nf^2(Q)}{Nf^2(Q)}\right] Q^2 dQ}{\int_0^{Q_{max}} \frac{I^{samp}}{Nf^2(Q)} Q^2 dQ}. \tag{6}$$

However equation (6) is exact only when $Q_{max} = \infty$ and this, coupled to the lack of knowledge of the liquid density, leads to an erroneous determination of the normalization factor. On the other hand, an accurate experimental determination of the scale factor, s , is made difficult due to the weakness of the sample signal in comparison to the background. Fortunately, the important conclusion of our method of analysis[20] is that an iterative optimization procedure can be used to reduce the uncertainty in α and in s. This method implies that the scale factor and the normalization factor are independent which was satisfied in our proof of principle experiments[20] and is also valid here. Surprisingly, there is a unique well-defined minimum in the figure of merit of the optimization and the density can also be estimated. It is based on a method developed by Kaplow et al.[24] using the fact that the theoretical form of F(r) is known below the first intermolecular peak: $F^{theo}(r) = -4\pi r\rho_0 + F_{intra}(r)$ for $r < r_{min}$. The term $F_{intra}(r)$ is the intra-molecular contribution to F(r). We assume in our analysis that the intra-molecular distance is frozen (d_{O-O}=1.2074 Å). The structure factor and the radial distribution function can then be iteratively improved by applying the following equations:

$$\begin{aligned}
&1)\ \ F_{(i)}(r) = \frac{2}{\pi}\int_0^{Q_{max}} Q i_{(i)}(Q)\sin(Qr)dQ \\
&2)\ \ \Delta F_{(i)}(r) = F_{(i)}(r) - [-4\pi r\rho_0 + F_{intra}(r)] \\
&3)\ \ i_{(i+1)}(Q) = i_{(i)}(Q) - \frac{1}{Q}\left[\frac{i_{(i)}(Q)f^2(Q)}{f^2(Q)I^{incoh}(Q)} + 1\right] \\
&\qquad\qquad \times \int_0^{r_{min}} \Delta F_{(i)}(r)\sin(Qr)dr.
\end{aligned} \tag{7}$$

The liquid density is in general not known. But ρ_0 is related to the normalization factor α through equation (6), so that α and ρ_0 can be simultaneously determined by minimizing $\chi^2_{(i)} = \int_0^{r_{min}} \Delta F^2_{(i)}(r) \sin(Qr) dr$. The procedure is then applied to determine the scale factor. Two iterations were generally sufficient for convergence. We have shown, and it is also the case here, that $S(Q)$ is relatively unaffected by the Qmax-cutoff problem. Measurements have been performed up to 90 nm^{-1}. The consequence on g(r) is that the intermolecular peaks are broadened but their position almost unchanged.

The X-ray diffraction experiments were performed up to the maximum pressure and temperature of 24 GPa and 750 K. 12 diffraction patterns were measured in two runs. In figure 3, two analyzed S(Q) are compared, the first, corresponding to the lowest density data point (P=7.4 GPa, T=357 K) and the other to the highest density one (P=17.2 GPa, T=750 K). The shapes of both structure factors are characteristic of a simple liquid with a ratio between the first and the second peak position in between 2.0 and 2.1. There is also no evidence of an intermediate peak around 40 nm^{-1} in the structure factor as reported in fluid oxygen at 77 K and ambient pressure[25] which had been interpreted as a signature of preferential orientation of nearest-neighbor molecules. Also, no critical change of the structure factor is observed over our domain of investigation. The main difference between the two S(Q) lies in the first peak position that shift to higher Q with pressure. Transformed into the radial distribution function g(r), that gives a g(r) for fluid oxygen very similar to the one of a fluid with weak molecular orientational correlation and the effect of pressure is characterized by a slight shift of the first intermolecular peak position to lower distances. A more detailed analysis of the evolution of the pair distribution function is given below through a comparison with a molecular dynamic simulation.

VI. DISCUSSION

In our domain of study, Raman and x-ray diffraction measurements have shown that fluid O_2 remains molecular, with weak change of the intramolecular bonding and weak orientational correlation between molecules. To try to quantify an effect of possible orientational correlation under pressure in fluid oxygen, we have compare the present g(r) data to the molecular dynamic simulation. The simulation has been performed in the (N,V,E) ensemble by chosing an exp-6 pair potential interaction adjusted on the Hugoniot curve of fluid

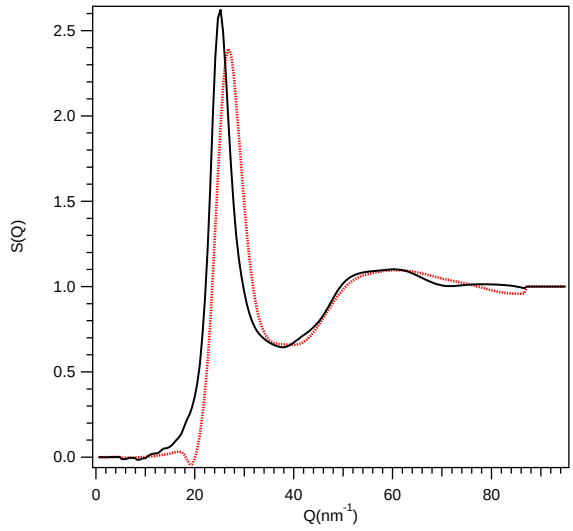

FIG. 3: Structure factor measured at T=357 K, P= 7.4 GPa (straight line) and at T=750 K, P=17.2 GPa (dot line).

oxygen (with $\alpha = 13$, $\varepsilon = 125$ and $r^\star = 3.84$ Å[26]). The simulations were done for density in between 63 mol/cm^3 and 90 mol/cm^3 and temperature from 300 K to 800 K. The time step was fixed to 10^{-15}s. The pressure was calculated with the Virial theorem and the radial distribution function was determined at each time step.

The simulation provides the molecule-molecule radial distribution function ($g_{O_2-O_2}$). In order to extract the atom-atom radial distribution function (g_{o-o}), we need to determine the atom distribution in the O_2 molecule. The molecular bond was described by an harmonic oscillator with a bond length d_{OO}=1.2074 Å and a vibration frequency $\nu = 1580.4\,\mathrm{cm}^{-1}$ corresponding to the gas phase value. For the harmonic oscillator, the repartition function is given by

$$w_{int}(r) = \frac{\sum_i |\phi_i(r)|^2 \exp(-E_i/k_BT)}{\sum_i \exp(-E_i/k_BT)}, \tag{8}$$

where $\phi_i(r)$ and E_i are respectively the eigenfunction and eigenvalue of the oscillator. Only the ground state is taken into account to calculate $w(r)$ (at 750 K the first and the second excited state represent respectively 4.8% and 0.3% of the occupation probability). The atom-atom pair distribution function is then given by

$$g_{o-o}(r) = \frac{1}{2n_{\mathrm{O}}} w_{int}(r) + \int d^3 s_1 \int d^3 s_2 w_{int}(\mathbf{s}_1) w_{int}(\mathbf{s}_2) \times g_{\mathrm{O_2-O_2}}(\mathbf{r} - \mathbf{s}_1/2 - \mathbf{s}_2/2), \quad (9)$$

where n_{O} is the number of atom by unit volume.

An illustrative comparison between the experimental derived radial distribution function g(r) and the one obtained from the MD simulation is shown at 17.2 GPa and 750 K in figure 4. The first peak in the experimental g(r) corresponds to the intramolecular O-O distance fixed at 1.2074 Å for the iterative analysis procedure (our experimental data cannot provide information on the internal structure of the oxygen molecule). The broadening of this peak is the result of the signal cutoff. This peak is not present in the MD simulated g(r) because the simulation is based on an intermolecular interaction, hence given for r-value greater than 0.185 nm. There is a relatively good agreement between the experimental and calculated g(r). However, we can see that the position of the first peak in the simulation is at a greater distance than in the experiment. That is observed for all the P-T domain covered here, as quantified in figure 5. Also, the first peak of the simulation is slightly more symmetric than the experimental one. That could indicate that the approximation of a spherical intermolecular interaction is not entirely valid.

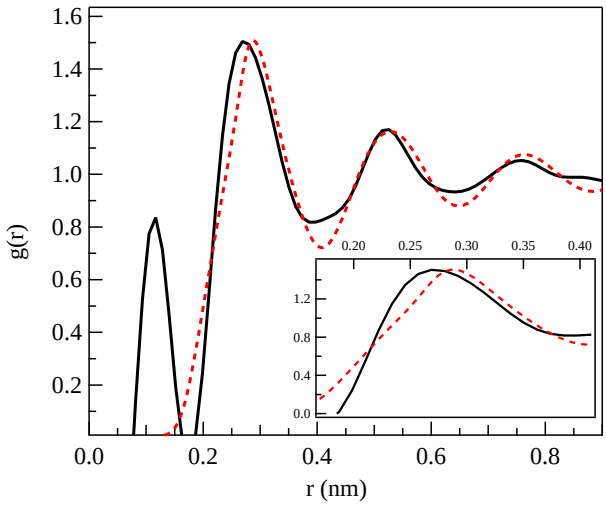

FIG. 4: Comparison between the experimental (straight line) and the MD simulated g(r) (dashed line) at 17.2 GPa and 750 K.

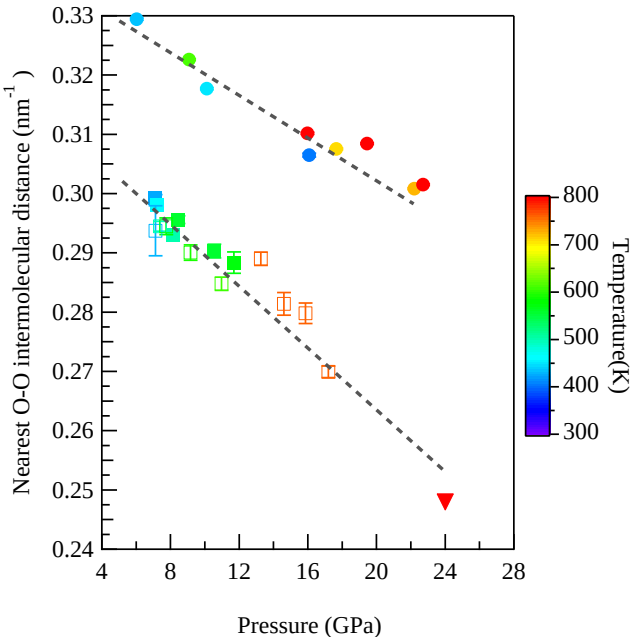

FIG. 5: Evolution of the first intermolecular O-O distance with pressure. Open and full squares represent two experiments. Circles and triangle correspond respectively to the classical and to the ab-inito[8] MD simulations. The dashed lines serve as guides for eyes. The temperature scale is given by the colors.

To determine the position of the intermolecular distance (d_{O-O}), we fit the first peak of the function $\sigma(r)=4\pi r^2\rho(g(r)-1)$ with a gaussian function. The function $\sigma(r)$ is preferred to the function g(r) because the shape of the intermolecular peak is more symmetric. The evolution with pressure and temperature of the first intermolecular distance is presented in figure 5. The scattering of the data is larger than the temperature effect on the peak position. On the other hand, we clearly observe the decrease of the O-O intermolecular distance with pressure. We also compare the experimental results to the molecular dynamic simulation. As seen on the radial distribution function, the O-O distance measured in the experiment is smaller than the one calculated in the simulation and the difference between both is larger than the uncertainties. More precisely, the difference (7 %) would correspond to a 21 % difference in volume. This is much larger than the difference (3%) between the volume calculated with an empirical EOS based on MD simulations performed with an exp-6 potential[19] and the one obtained from speed of sound measurements[27]. Hence, this difference should be attributed to a partial orientational correlation of the molecules.

Recently, ab-initio calculation has been performed on fluid oxygen at high pressure and high temperature[8]. The position of the first intermolecular peak calculated at P=24 GPa and T=1000K is shown as a large triangle in figure 5 and it is in very good agreement with the extrapolation of our measurement. It somehow validates the present measurement of the evolution of g(r) with pressure. At P=24 GPa and T=1000K, the ab-initio calculation predicts that fluid oxygen is purely formed of O_2 molecules. The association under pressure of the O_2 molecules into an O_8 unit has been observed in the solid phase when the nearest neighbor distance between O_2 molecules gets to 2.34 Å. Based on the extrapolation in figure 5 such a distance would be obtained in this fluid for a pressure in between 30 and 40 GPa. That is certainly a motivating issue to extend the present measurements at higher pressure.

VII. CONCLUSION

We have performed the first measurements of the structure factor of a low-Z molecular fluid under high pressure. It is the first application of a recently published method of analysis to extract the coherent x-ray scattering intensity from a fluid sample in a DAC. A quantitative structural information is obtained here, namely the decrease of the nearest O-O intermolecular distance with pressure. An interesting speculation is made by extrapolating this curve. If any, the molecular association of O_2 in the fluid phase would require pressures in the 40 GPa range to be observed. Also structural study at the insulating/conducting transition in fluid oxygen would require pressure in the 100 GPa range. That is a very challenging measurement not impossible though with the present approach. Finally, the same measurements should now be performed on other low-Z systems, H_2O, N_2 and CO_2, with interesting issues for planetary interiors.

Acknowledgments

We acknowledge the European Synchrotron Radiation Facility for provision of synchrotron radiation facilities. J. Eggert would like to thank CEA for a 2000-2002 visitor

program during which the structural study method was implemented.

This work was performed under the auspices of the DOE by UC, LLNL under Contract W-7405-Eng-48.

[1] I. Goncharenko and P. Loubeyre, Nature (London) **435**, 1206 (2005).

[2] L. F. Lundegaard, G. Weck, M. I. McMahon, S. Desgreniers, and P. Loubeyre, Nature (London) **443**, 201 (2006).

[3] M. I. Eremets, A. G. Gavriliuk, I. A. Trojan, D. A. Dzivenko, and R. Boehler, Nature Materials **3**, 558 (2004).

[4] M. Santoro, F. A. Gorelli, R. Bini, G. Ruocco, S. Scandolo, and W. A. Crichton, Nature (London) **441**, 857 (2006).

[5] M. Bastea, A. C. Mitchell, and W. J. Nellis, Phys. Rev. Lett. **86**, 3108 (2001).

[6] R. Chau, A. C. Mitchell, R. W. Minich, and W. J. Nellis, Phys. Rev. Lett. **90**, 245501 (2003).

[7] F. Datchi and B. Canny, Phys. Rev. B **69**, 144106 (2004).

[8] B. Militzer, F. Gygi, and G. Galli, Phys. Rev. Lett. **91**, 265503 (2003).

[9] T. Oda and A. Pasquarello, Phys. Rev. Lett. **89**, 197204 (2002).

[10] F. Datchi, P. Loubeyre, and R. Letoullec, Phys. Rev. B **61**, 6535 (2000).

[11] F. Datchi, R. Letoullec, and P. Loubeyre, J. Appl. Phys. **81**, 3333 (1997).

[12] A. Hammersley, ESRF publication No. ESRF98HA01T (1996).

[13] G. Monaco, S. Falconi, W. A. Crichton, and M. Mezouar, Phys. Rev. Lett. **90**, 255701 (2003).

[14] M. Santoro, E. Gregoryanz, H.-K. Mao, and R. J. Hemley, Phys. Rev. Lett. **93**, 265701 (2004).

[15] R. LeToullec, F. Datchi, P. Loubeyre, N. Rambert, B. Sitaud, and T. Thévenin, in *High-Pressure Science and Technology* (1996), p. 54.

[16] J. Yen and M. Nicol, J. Phys. Chem. **91**, 3336 (1987).

[17] M. Nicol, K. R. Hirsch, and W. B. Holzapfel, Chem. Phys. Lett. **68**, 49 (1979).

[18] Y. Akahama and H. Kawamura, Chem. Phys. Lett. **400**, 326 (2004).

[19] A. Belonoshko and S. K. Saxena, Geochim. Cosmochim. Acta **55**, 3191 (1991).

[20] J. H. Eggert, G. Weck, P. Loubeyre, and M. Mezouar, Phys. Rev. B **65**, 174105 (2002).

[21] F. Hajdu, Acta Cryst. **A28**, 250 (1972).

[22] J. Krogh-Moe, Acta Cryst. **9**, 951 (1956).

[23] N. Norman, Acta Cryst. **10**, 370 (1957).

[24] R. Kaplow, S. L. Strong, and B. L. Averbach, Phys. Rev. **138**, A1336 (1965).

[25] J. Dore, G. Walford, and D. Page, Mol. Phys. **29**, 565 (1975).

[26] M. Ross and F. H. Ree, J. Chem. Phys. **73**, 6146 (1980).

[27] E. H. Abramson, L. J. Slutsky, M. D. Harrell, and J. M. Brown, J. Chem. Phys. **110**, 10493 (1999).